inter.noise
27-30 AUGUST HONG KONG 2017

Noise radiation from an AC filter capacitor

Jiancheng TAO[1]; Jiaxin ZHONG[2]; Xiaojun QIU[3]

[1] Key Laboratory of Modern Acoustics and Institute of Acoustics, Nanjing University, Nanjing, China

[2] Key Laboratory of Modern Acoustics and Institute of Acoustics, Nanjing University, Nanjing, China

[3] Centre for Audio, Acoustics and Vibration, Faculty of Engineering and IT, University of Technology Sydney, Australia

ABSTRACT

Numerous alternating current (AC) filter capacitors are used on the AC side in the high-voltage direct-current transmission systems, and therefore their noise is one important contributor to the total noise in converter stations. In this paper, the noise radiation and the vibration information of an AC filter capacitor is measured and analyzed with multi harmonic excitations. A boundary element model for the noise radiation prediction is established and validated using the measurement data under a typical excitation condition. Based on the prediction model, the noise contribution of different surfaces of the capacitor is calculated. It is found that the top surface and one broad surface are major contributors to the sound power peaks, and the sound power level of the capacitor can be reduced by 7.5 dB, 6.7 dB, 7.8 dB and 5.0 dB respectively at 100 Hz, 500 Hz, 600 Hz and 700 Hz when the vibration at these two surfaces is completely suppressed.

Keywords: Capacitor noise I-INCE Classification of Subjects Number(s): 12

1. INTRODUCTION

Hundreds of alternating current (AC) filter capacitors are employed in the high-voltage direct-current converter stations for power-factor correction. It has already been reported that the near field noise level around the filter capacitor stacks nearly equals to that around the power transformers or smoothing reactors, especially when the input current consists of high order harmonic components (1).

The vibration and audible noise of capacitors subjected to nonsinusoidal current was firstly investigated in 1994, and it was found that significant high frequency vibration occurs due to the attractive force when the input current is distorted (2). In the following studies, the sound power of the filter capacitor was typically formulated by multiplying the vibration power by a radiation efficiency factor (3). Therefore accurate estimation of the vibration velocity of the capacitor becomes the main issue in the capacitor noise prediction. Both the mechanical and electro-mechanical frequency response functions were proposed to predict the vibration velocity and the sound power of the capacitors (4, 5). Recently, the noise characteristics of the filter capacitors were analyzed by using both theoretical and boundary element models, and the effects of vibration frequency, phase angle and magnitude of the input voltage on the sound radiation of the capacitors were investigated (6). Besides, possible solutions to reduce the capacitor noise were also investigated (7, 8, 9).

In this paper, the vibration and sound radiation of an AC filter capacitor with harmonic current excitations is investigated. Firstly, the sound power level of the capacitor excited by different input currents is measured and analyzed. Next, the fitting formula are proposed based on the measured sound power level to directly predict the sound power level at 500 Hz, 600 Hz and 700 Hz with different exaction magnitudes. Then a boundary element model is built to calculate the sound power with a typical excitation configuration. Finally, the noise radiation contribution of the capacitor surface is discussed using the boundary element

[1] jctao@nju.edu.cn
[2] jxzh@smail.nju.edu.cn
[3] xiaojun.qiu@uts.edu.au

model.

2. Theory

Fig. 1 shows the outer shell and inner elements of the AC capacitor investigated in this paper. The outer shell of the capacitor is an enclosed hexahedral box made by steel plates, and two bushings are installed on the top surface. The length, width and height of the capacitor is 1070 mm, 380 mm and 200 mm respectively, and the thickness of shell is within 1~ 2 mm. The inner elements of the capacitor are made by winding aluminum foils and plastic films, and all the elements are immersed within a dielectric fluid contained by the outer shell.

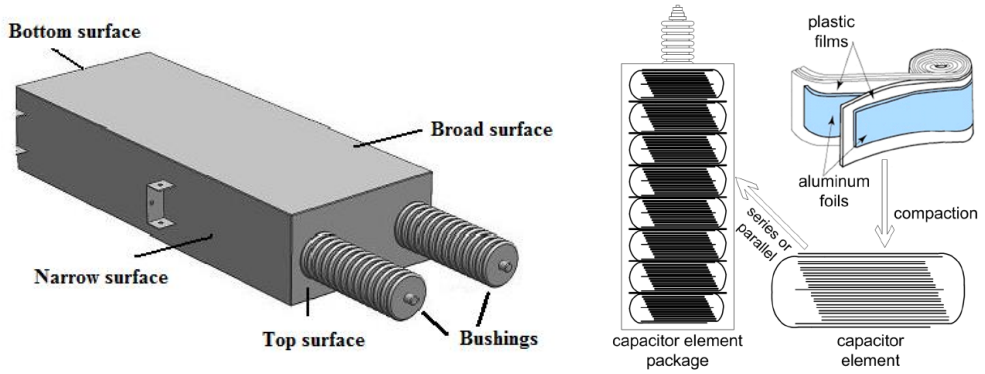

(a) (b)

Figure 1 – Sketch map of the AC filter capacitor (a) outer shell (b) inner elements

2.1 Force analysis

When the AC current is applied on the capacitor, all aluminum foils are energized and nearly all plastic films are in force. This time-varying attractive force excites the outer shell to vibrate through both the dielectric fluid and the connectors between the capacitor elements and the outer shell, and thus the noise generates. The attractive force per area is (2)

$$F(f)=\frac{1}{2}\varepsilon\left(\frac{u}{d}\right)^2=\frac{1}{2}\varepsilon\left(\frac{I}{2\pi fCd}\right)^2=K(f)I^2, \tag{1}$$

where ε is the dielectric constant of the dielectric fluid, d is the distance between the electrode plates of the capacitor, u is the voltage applied on the capacitor, I is the input current, C is the value of the capacitor, f is the frequency of the input voltage or current, and the coefficient $K(f)=\varepsilon/8\pi^2 f^2C^2d^2$. Eq. (1) shows that the attractive force is proportional to the square of the input current; therefore the induced vibration of the outer shell and the reradiated sound pressure level will be enhanced by 12 dB when the magnitude of a sinusoidal input current is doubled.

In practical implementation, the input current may consist of high order harmonics. Assuming that the input current is composed of a fundamental frequency component and an nth order harmonic component with the same phase angle, the input AC current can be formulated as

$$I(t)=I_1\sin\omega t+I_n\sin n\omega t, \tag{2}$$

where ω is angular frequency corresponding to the power frequency, I_1 and I_n is the magnitude of the fundamental and nth order harmonic current respectively, t is the time variable. Substituting Eq. (2) into Eq. (1), it is be obtained that

$$F(t)=\frac{1}{2}K_1^2I_1^2(1+\cos 2\omega t)+\frac{1}{2}K_n^2I_n^2(1+\cos 2n\omega t)+K_1K_nI_1I_n\cos[(n+1)\omega t]+K_1K_nI_1I_n\cos[(n-1)\omega t]. \tag{3}$$

It is clear that a frequency modulation occurs as shown in Fig. 3. Four different frequency components, the 2ω component, the $2n\omega$ component, the $(n\text{-}1)\omega$ component, and the $(n\text{+}1)\omega$ component will be generated in the attractive force when the input current consists of 2 harmonic components. Eq. (3) also shows that the force magnitude of the 2ω and $2n\omega$ components is determined by the magnitude I_1 and I_n respectively; however, the force magnitude of the $(n\text{-}1)\omega$ and the $(n\text{+}1)\omega$ components are dependent on both I_1 and I_n. If

the capacitor is considered as a linear system, the attractive force, the vibration response and the sound pressure level of the $(n\text{-}1)\omega$ and $(n\text{+}1)\omega$ components will be enhanced by 6 dB when I_1 is fixed and I_n increases to 2 times.

2.2 Sound radiation calculation

In most investigations on the audible noise of capacitors, the sound power of the capacitor, W_{rad}, is typically calculated using

$$W_{\text{rad}} = \rho_0 c S v^2 \sigma \tag{4}$$

where ρ_0 is the air density, c is the sound speed in air, S is the total area surrounding the AC filter capacitor, v is the average velocity over the capacitor surface and σ is the radiation efficiency factor. Obviously, Eq. (4) is obtained from the energy concept and cannot be used to calculate the detailed radiation pattern of the sound pressure surround the capacitor.

A more accurate method to predict the sound radiation is using the boundary element method which taking both the magnitude and the phase of the velocity into account. For the capacitor investigated in this paper, the boundary element model built in SYSNOISE 5.6 is presented in Fig. 2, where a enclosed hexahedral box is adopted to simulate the outer shell of the capacitor and the brushings are neglected. Considering the semi-anechoic condition in the experiments, a rigid reflecting plate (5 m × 5 m) is also added 0.8 m below the box. If the velocity over the box is input as the boundary condition, the sound pressure at any point above the reflecting plate can be calculated, and then the sound power level can also be calculated using the averaged sound pressure level at 9 positions according to the standard GB/T 32524.2-2016 (10).

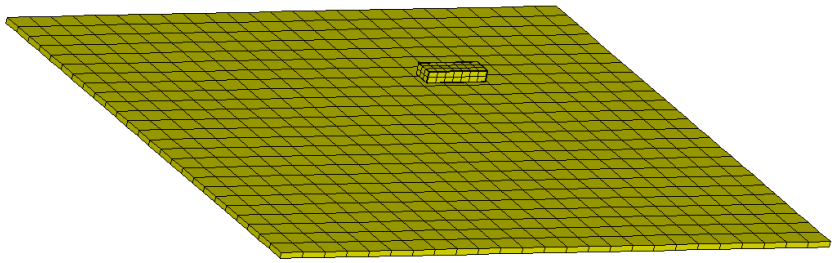

Figure 2 – Boundary element model of the AC filter capacitor in a semi-anechoic chamber

3. Experiment measurements

Both the sound radiation and the vibration velocity of the AC filter capacitor were measured in a semi-anechoic chamber using the multichannel analyzer B&K 3560B. During the sound radiation measurement, 6 different input currents are applied and the detailed excitation configurations are listed in Table 1, where the fundamental frequency is 50 Hz.

Table 1 – Configurations of input current

Configuration	Fundamental component magnitude (A)	Harmonic components order /magnitude (A)
T1	65.865	11/11.385, 13/36.305
T2	65.865	11/14.801, 13/47.197
T3	65.865	11/5.693, 13/18.153
T4	65.865	11/3.416, 13/10.892
T5	79.000	5/1, 7/2, 11/31, 13/21
T6	59.260	9/11.490, 11/54.125

The sound pressure level and sound power level measured with different excitation configurations is shown in Fig. 3. Fig. 3(a) shows that the background noise mainly appears at frequencies below 200 Hz. Considering the background noise, the measured noise level peaks occur at 100 Hz, 500 Hz, 600 Hz and 700 Hz with the excitation T1 as shown in Fig. 3(b). The excitation T1 consists of 50 Hz, 550 Hz and 650 Hz components and therefore the force should have components at 100 Hz, 500 Hz, 600 Hz, 700 Hz, 1100 Hz, 1200 Hz and 1300 Hz theoretically according to Eq. (3). The reason that no obvious noise peaks are measured at 1100 Hz, 1200 Hz and 1300 Hz may due to the damping provided by the dielectric fluid. The noise peaks in Figs. 3(c) and 3(d) also present the same frequency modulation characteristics as shown in Fig. 3(b).

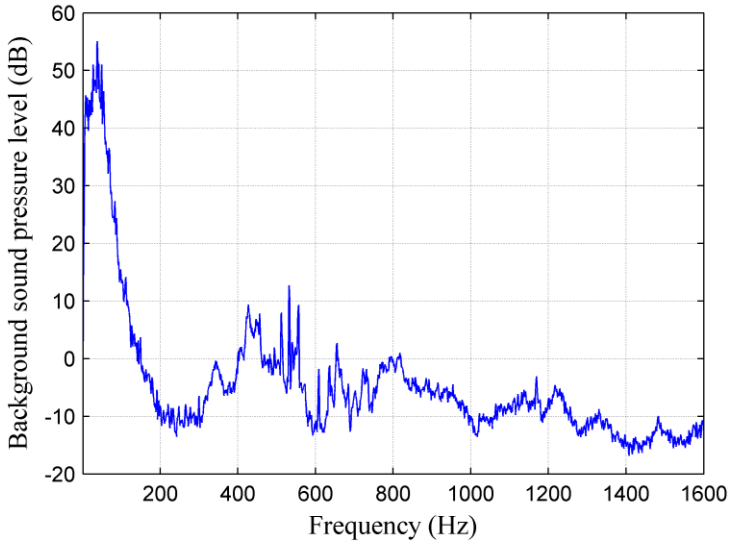

(a)

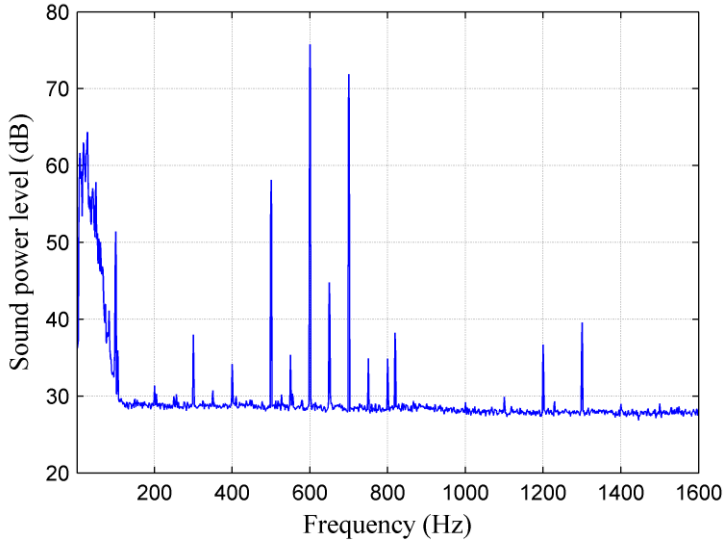

(b)

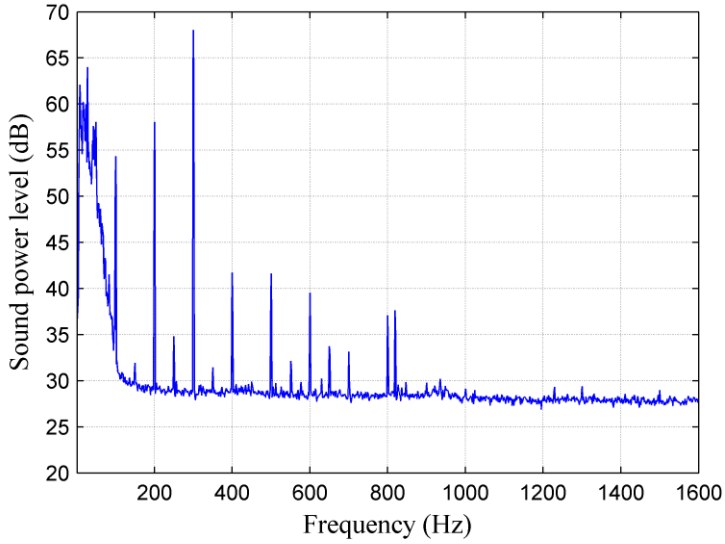

(c)

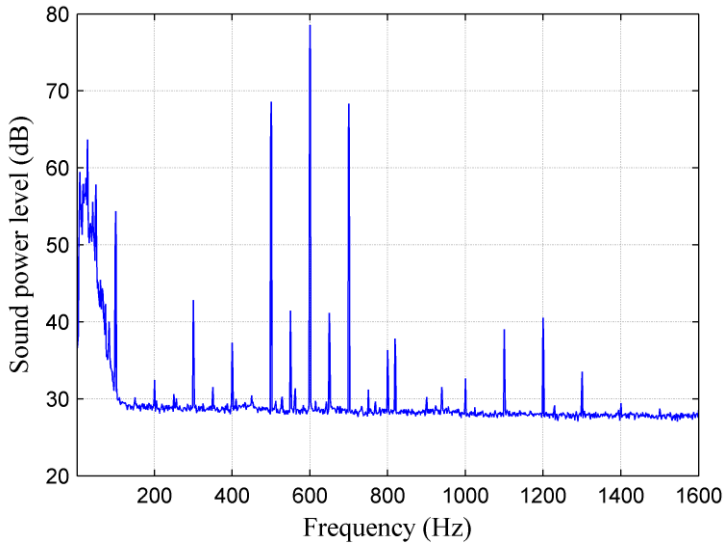

(d)

Figure 3 – Measured sound pressure level and sound power level of the AC filter capacitor (a) background noise (b) sound power level with T1(c) sound power level with T5 (d) sound power level with T6

Among all the excitation configurations, T1 ~ T4 are typical excitation configurations (the input current consists of the fundamental component, the 11th order component and 13th order component, but the magnitude of each component may vary) in a real converter station. The vibration distribution at 134 surface positions, which correspond to the nodes of the boundary element model in Fig. 2, was also measured as shown in Fig. 4. To distinguish the surfaces clearly, the capacitor surfaces are named as surface A1~A6. The interval of the measurement positions is 150 mm, 120 mm and 90 mm in the length, width and height directions respectively. During the measurement, an accelerometer (PCB 333B31) is fixed at the position 255, and other 13 accelerometers are placed at different positions to measure the magnitude and the phase angle of the vibration velocity one time. Considering the total number of the measurement positions, the accelerometers except the fixed one were removed to different positions 11 times.

(a)

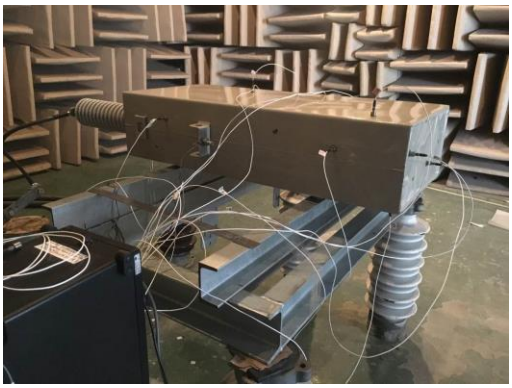

(b)

Figure 4 – Experimental setup for vibration measurement (a) measurement positions (b) measurement photo

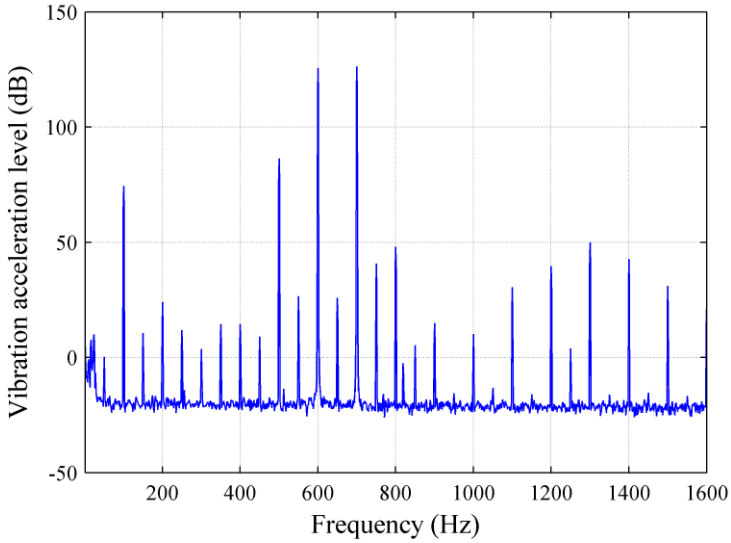

Figure 5 – Measured acceleration level at the position 235 with the excitation T1

The measured normal acceleration level at the position 235 with the excitation T1 is shown in Fig. 5, where the acceleration at 100 Hz, 500 Hz, 600 Hz and 700 Hz is 10 dB higher than the peaks at 1100 Hz and 1300 Hz. The first reason for this level difference may due to the damping of the dielectric fluid as

mentioned above. The second reason is that the coefficient $K(f)$ is inversely proportional to the frequency, and therefore the attractive force is smaller around 1100 Hz and 1300 Hz. Because the acceleration level at 1100 Hz and 1300 Hz is sufficiently low compared to the values at 500 Hz, 600 Hz and 700 Hz, there is no obvious noise peak at 1100 Hz and 1300 Hz in the spectrum of the sound power level in Fig. 3 (b).

4. Discussions

4.1 Direct prediction of the sound power peaks

According to Eqs. (1) and (3), the attractive force increases with the magnitude of the input current. Assuming the capacitor as a linear system and considering the excitation configurations in Table 1, the level of the sound power peaks can be formulated using the fitting formula as

$$\mathrm{SWL}_{500\mathrm{Hz}} = 20\log\left(A_1 I_1 I_{11}\right) \quad \text{with T1} \sim \text{T5}, \tag{5a}$$

$$\mathrm{SWL}_{600\mathrm{Hz}} = \begin{cases} 20\log\left(A_2 I_1 I_{11} + A_3 I_1 I_{13}\right) & \text{with T1} \sim \text{T4} \\ 20\log\left(A_2 I_1 I_{11}\right) & \text{with T6} \end{cases}, \tag{5b}$$

$$\text{and} \qquad \mathrm{SWL}_{700\mathrm{Hz}} = 20\log\left(A_4 I_1 I_{13}\right) \quad \text{with T1} \sim \text{T5}, \tag{5c}$$

where $\mathrm{SWL}_{500\mathrm{Hz}}$, $\mathrm{SWL}_{600\mathrm{Hz}}$ and $\mathrm{SWL}_{700\mathrm{Hz}}$ is the sound power level at 100 Hz, 500 Hz, 600 Hz and 700 Hz respectively, I_1, I_9, I_{11}, I_{13} is the magnitude of the fundamental, the 9th order harmonic, the 11th order harmonic and the 13th order harmonic in the input current respectively, A_1, A_2, A_3 and A_4 are the coefficients to be determined. Substituting the measured sound power level at these frequencies and the magnitude of the input current into Eq. (5), the coefficients can be calculated as $A_1 = 1.0456$, $A_2 = 0.029$, $A_3 = 2.53$, $A_4 = 1.6261$ respectively. Therefore, if the capacitor works with the typical excitations, the sound power level at 500 Hz and 700 Hz can be predicted using

$$\mathrm{SWL}_{500\mathrm{Hz}} = 20\log\left(1.0456 I_1 I_{11}\right), \tag{6a}$$

$$\mathrm{SWL}_{600\mathrm{Hz}} = 20\log\left(0.029 I_1 I_{11} + 2.53 I_1 I_{13}\right), \tag{6b}$$

$$\text{and} \qquad \mathrm{SWL}_{700\mathrm{Hz}} = 20\log\left(1.6261 I_1 I_{13}\right). \tag{6c}$$

The predicted sound power level at 500 Hz and 700 Hz using Eq. (6) is shown in Fig. 6, where the predicted results agree well with the measured data. The sound power level at 600 Hz is not presented in Fig. 6 because the sound power level is contributed by two terms at 600 Hz according to Eq. 6 (b) and cannot be simply predicted using one parameter $I_n I_m$ as the x-axis label in Fig. 6.

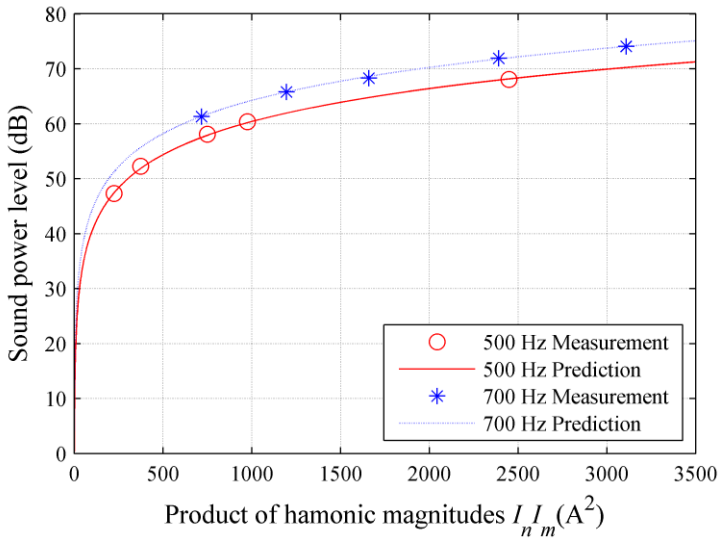

Figure 6 – Predicted and measured sound power level at 500 Hz and 700 Hz with different excitations

4.2 Accuracy of the boundary element model

If the measured velocity is input into the boundary element model shown in Fig. 2 as the boundary condition, the sound pressure level above the reflecting surface and the sound power level can be calculated. The calculated sound pressure level at one measurement microphone with the excitation T1 is shown in Fig.

7(a), where the level difference at 100 Hz, 500 Hz, 600 Hz and 700 Hz is 1.3 dB, 0.5 dB, 0.7 dB and 1.2 dB respectively. The calculated sound power level with the excitation T1 is shown in Fig. 7 (b), where the level difference is 0.2 dB, 0.7 dB, 2.4 dB and 0.3 dB at 100 Hz, 500 Hz, 600 Hz and 700 Hz respectively. Fig. 7(a) also shows that the difference between the measured and calculated results is over 20 dB except the main noise peaks. This large difference may be caused by two reasons. The first reason is that the background noise of the semi-anechoic chamber is large at these frequencies. The second reason is that the noise radiation from the bushings and support frame is not considered in the boundary element model.

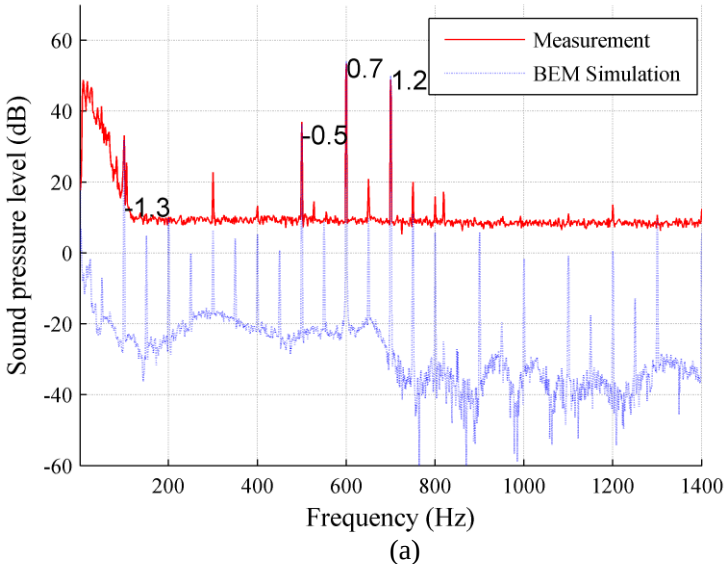

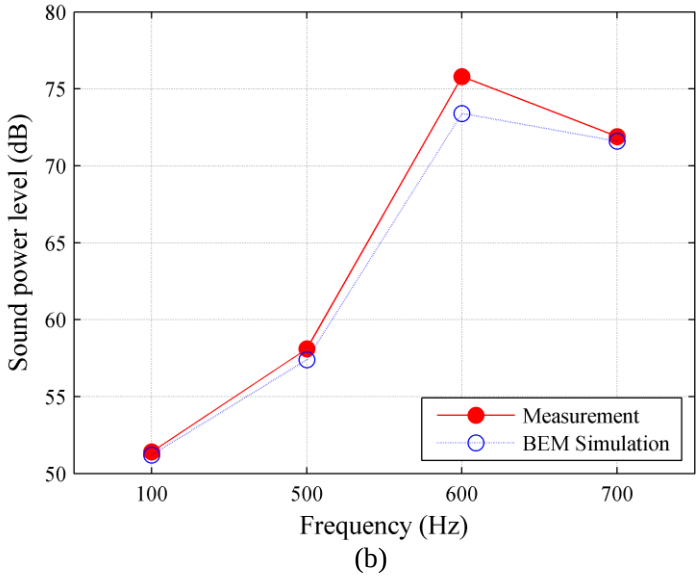

Figure 7 – Calculated results based on the boundary element model (a) the sound pressure level at one randomly chosen microphone (b) the sound power level at 100 Hz, 500 Hz, 600 Hz and 700 Hz.

Based on the calculation results, it is validated that the boundary element model is accurate to calculate the main noise peaks using the velocity distribution measured according to the setup shown in Fig. 4(a). However, the boundary element model needs to be further improved to accurately calculate the noise at other frequencies.

4.3 Noise contribution from different surfaces

The measured normal velocity level over the capacitor surfaces at 100 Hz, 500 Hz, 600 Hz and 700 Hz with excitation T1 is presented in Fig. 9, where it is obvious that the maximum vibration always appears at

the top surface. This indicates that the vibration transmits to top surfaces easily through the connections between the inner capacitor elements and the outer shell.

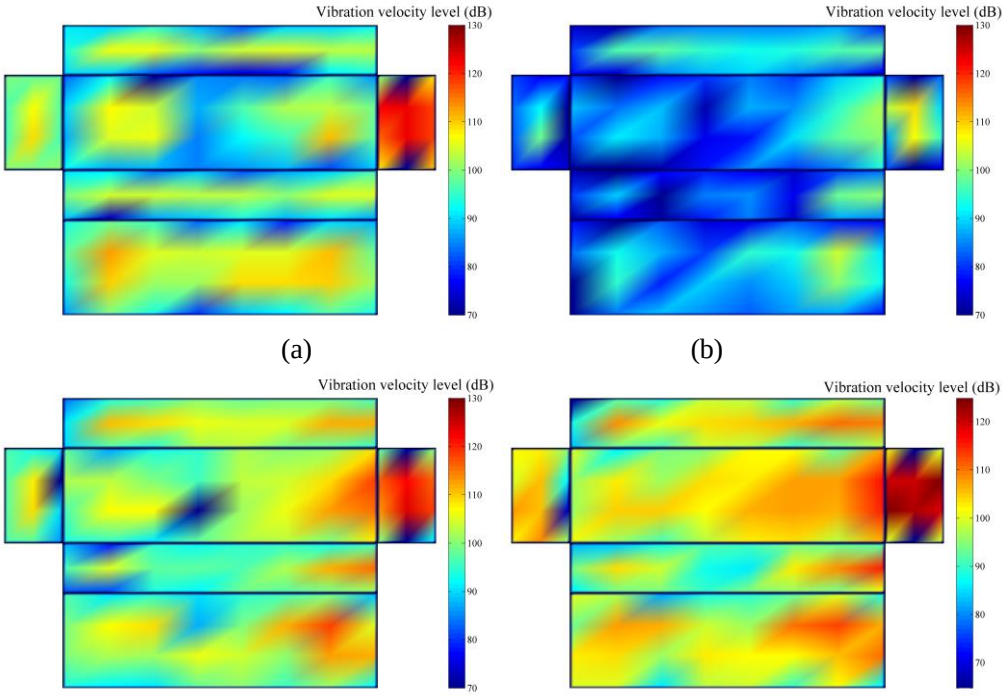

Figure 9 – Measured velocity level over the capacitor surfaces (a) 100 Hz (b) 500 Hz (c) 600 Hz (d) 700 Hz

The contribution of one measurement position on the total sound power level, ΔL_i, can be calculated as

$$\Delta L_i = \mathrm{SWL}_0 - \mathrm{SWL}_i \tag{6}$$

where SWL_0 is the calculated sound power level using all the measured velocity, SWL_i is the calculated sound power level by setting the velocity at the *i*th position to zero and inputting the measured velocity at other positions. The distribution of this contribution at 100 Hz, 500 Hz, 600 Hz and 700 Hz is shown in Fig. 10, where the top surface A5 and the broad surface A2 are major contributors to the total sound power level at these peak frequencies.

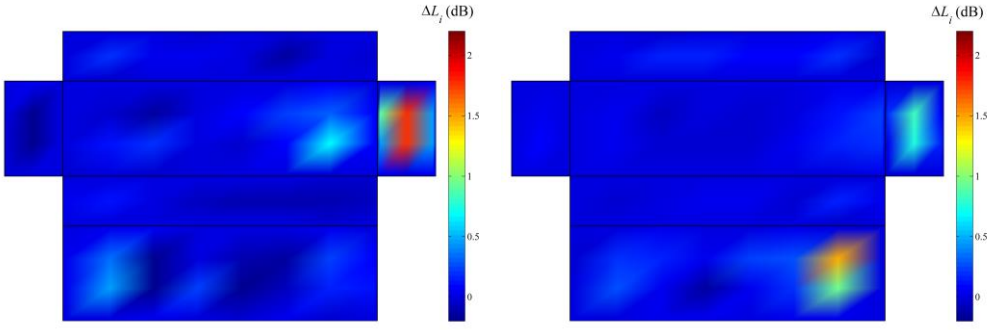

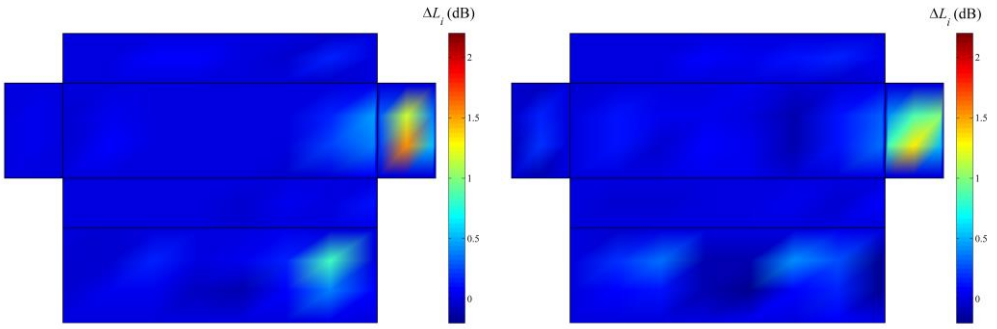

(c) (d)

Figure 10 – Calculated sound power contribution over the capacitor surfaces (a) 100 Hz (b) 500 Hz (c) 600 Hz (d) 700 Hz

If the vibration over the top surface A5 and the broad surface A2 can be completed suppressed, the calculated sound power level using the boundary element model is presented in Fig. 11. Fig.11 indicates that if the vibration on surface A5 is completely suppressed, the noise reduction at 100 Hz, 500 Hz, 600 Hz and 700 Hz is 5.3 dB, 1.7 dB, 3.0 dB and 3.9 dB. If the vibration on surface A2 is completely suppressed, the corresponding noise reduction is 0.8 dB, 2.9 dB, 0.8 dB and 0.7 dB. If the vibration on both A2 and A5 is completely suppressed, the corresponding noise reduction increases to 7.5 dB, 6.7 dB, 7.8 dB and 5.0 dB.

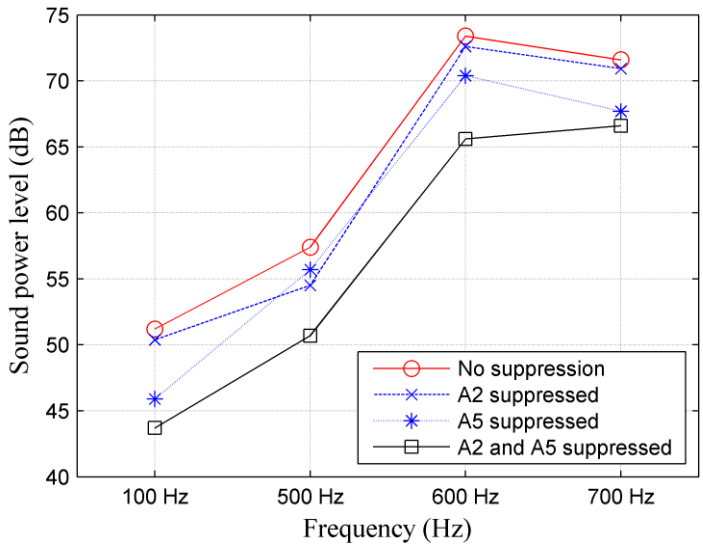

Figure 11 – Calculated sound power peaks when the surface vibration is completely suppressed

5. Conclusions

In this paper, the vibration and noise characteristics of an AC capacitor is investigated. Considering the frequency modulation of the attractive force, many harmonic components occurs in both vibration velocity and sound pressure, when a multi-harmonic current is applied. For the typical current input consisting of the fundamental component, the 11th order and 13th order components, a formulation is obtained by fitting the measured results to predict the sound power level at 500 Hz, 600 Hz and 700 Hz. Furthermore, an boundary element model was built to predict the noise spectrum of the capacitor, and the maximum prediction error of the sound power level is 2.4 dB when calculating the sound power level at 100 Hz, 500 Hz, 600 Hz and 700 Hz. It is also found that the top surface and one broad surface are major contributors to the sound power peaks, and the sound power level of the capacitor can be reduced by 7.5 dB, 6.7 dB, 7.8 dB and 5.0 dB respectively at 100 Hz, 500 Hz, 600 Hz and 700 Hz when the vibration at these two surfaces is completely suppressed.

ACKNOWLEDGEMENTS

This research was supported under the Australian Research Council’s Linkage Projects funding scheme (LP140100987) and by the National Science Foundation of China (11474163).

REFERENCES

1. HVDC stations audible noise, WG. 14.26 France, CIGRE Tech. Rep. 2002.
2. Cox MD, Guan HH. Vibration and audible noise of capacitors subjected to nonsinusoidal wave-forms. IEEE Transactions on Power Delivery 1994;9:856-62.
3. Smede H, Johansson C, Winroth O, Schutt H. Design of HVDC converter stations with respect to audible noise requirements. IEEE Transactions on Power Delivery 1995;10:747-58.
4. Ji SC, Wu P, Zhang QG, Li YM, Study on the noise-level calculation method for capacitor stacks in HVDC converter station. IEEE Transactions on Power Delivery 2010;25(3):1866-73.
5. Zhu LY, Ji SC, Shen Q, Liu Y, Li JY, Liu H. A noise level prediction method based on electro-mechanical frequency response function for capacitors. PloS one 2013; 8(12):e81651.
6. Zhu LY, Li JY, Shi YH, Rehman H, Ji SC. Audible noise characteristics of filter capacitors used in HVDC converter stations. IEEE Transactions on Power Delivery, 2016;PP(99):1-1.
7. Wu P, Ji SC, Li YM, Cao T. Study on an audible noise reduction measure for filter capacitors based on compressible space absorber. IEEE Transactions on Power Delivery 2011;26(1):438-45.
8. Wu P, Ji SC, Cao T, Li YM, Li XL, Li Y. Study on an audible noise reduction measure for the filter capacitors in the HVDC converter station based on the MPP absorber. IEEE Transactions on Power Delivery 2009;24(4):1756-62
9. Roget AB. Study of vibration and audible noise generated by shunt capacitor banks at substations serving non-linear loads. Master thesis, the University of Alabama; 2011.
10. GB/T 32524.2: Acoustics - Determination of sound power level and directivity character of power capacitor using sound pressure - Part 2 : Engineering methods for an essentially free field over a reflecting plane, Standardization Administration of the People's Republic of China; 2016.